

Non-uniform virtual material modeling on contact interface of assembly structure with bolted joints

Jianbin Cao^{1,2a}, Zhousuo Zhang^{*1,2}, Wenzhan Yang^{1,2b} and Yanfei Guo^{1,2c}

¹School of Mechanical Engineering, Xi'an Jiaotong University, Xi'an 710049, PR China
²State Key Laboratory for Manufacturing and Systems Engineering, Xi'an Jiaotong University, Xi'an 710049, PR China

(Received June 2, 2019, Revised July 2, 2019, Accepted July 15, 2019)

Abstract. Accurate modeling of contact interface in bolted joints is crucial in predicting the dynamic behavior for bolted assemblies under external load. This paper presents a contact pressure distribution based non-uniform virtual material method to describe the joint interface of assembly structure, which is connected by sparsely distributed multi-bolts. Firstly, the contact pressure distribution of bolted joints is obtained by the nonlinear static analysis in the finite element software ANSYS. The contact surface around bolt hole is divided into several sub-layers, and contact pressure in each sub-layer is thought to be evenly. Then, considering multi-asperity contact at the micro perspective, the relationship between contact pressure and interfacial virtual material parameters for each sub-layer is established by using the fractal contact theory. Finally, an experimental platform for the dynamic characteristics testing of a beam lap structure with double-bolted joint is constructed to validate the efficiency of proposed method. It is found that the theoretical results are in good agreement with experimental results by impact response in both time- and frequency-domain, and the relative errors of the first four natural frequencies are less than 1%. Furthermore, the presented model is used to examine the effect of rough contact surface on dynamic characteristics of bolted joint.

Keywords: bolted joints; rough contact surface; fractal contact theory; non-uniform virtual material

1. Introduction

Bolted joints are widely used for fastening two or more parts together to constitute a component in mechanical products and engineering structures due to their properties of high load-carrying capacity, low cost and ease of disassembly for maintenance (Ksentini *et al.* 2015). The presence of connection interface of bolted joints in a structure inevitably leads to cut down the overall stiffness and introduce additional energy dissipation, which would influence natural frequencies and vibration amplitudes of the structure (Abid and Khan 2013, Lopez-Arancibia *et al.* 2015). Moreover, rough surfaces at micro-scale make the contact mechanism more complex, and inaccurate modeling of bolted joints may cause unacceptable errors during dynamic analysis (Abad *et al.* 2012). Therefore, it is vital to investigate the joint interface modeling and construct an accurate model of bolted joints to determine the dynamic behavior of the structure.

In order to characterise a bolted joint, researchers have

been developed a series of interesting techniques. Kim *et al.* (2007) presented four kinds of three-dimensional finite element models for the bolted joints, which were verified by static experiment. Then the proposed model was utilized for structure analysis of the marine diesel engine. Gantry *et al.* (2011) and Ahmadian and Jalali (2007a) simplified the joint interface region of bolted joints as the lumped mass-spring system, where the springs and viscous dampers were applied to describe the connection stiffness and damping. Ahmadian and Jalali (2007b) developed a nonlinear generic element formulation to represent the bolted joint. Song *et al.* (2004) presented an adjusted Iwan beam element for dynamic analysis of beam lap structure with bolted joints. The adjusted Iwan model is composed of a parallel combination of spring-slider elements that exhibits nonlinear behavior. Because of its ability to simulate the elastic-plastic behavior of the joint interface, the Iwan's model has been extensively studied and discussed (Argatov and Bucher 2011, Mignolet *et al.* 2015, Brake 2017). In addition, dynamic parameters identification of bolted joints is also a widely studied technique (Iranzad and Ahmadian 2012, Mehrpouya *et al.* 2013, Heller *et al.* 2009), which is implemented through minimizing the discrepancy between measured frequency response function (FRF) and the predicted FRF. However, the methods mentioned above are suitable for modeling of simple structural systems, but not for complex structural system containing large amount of joints and high degrees of freedom (Adele *et al.* 2017). Furthermore, it is difficult to apply these approaches to describe the relationships between the dynamic characteristics of bolted joints and the pretension torque, surface roughness of joint interface, and material properties.

*Corresponding author, Professor
E-mail: zzs@mail.xjtu.edu.cn

^a Ph.D. Student
E-mail: jianbincao@163.com

^b Ph.D. Student
E-mail: 1367014188@qq.com

^c Ph.D. Student
E-mail: flyyanguo@126.com

Fractal contact theory can characterize the contact mechanism of rough surfaces at micro-scale, and the dynamic parameters of joint interface at macro-scale can be obtained by using elastic-plastic deformation of contact asperities and surface topography description. Greenwood and Williamson (1966) first presented the probability-statistical contact model for two rough contact surfaces known as the GW model, which is then further developed by other researchers (Kogut and Etsion 2002, Jackson and Green 2005). Majumdar and Bhushan (1991) determined the radius of curvature of the deformed asperity through the asperity wavelength and amplitude, and then exploited a fractal based description method for contact surface. Zhang *et al.* (2014) modified the method and derived the contact stiffness and damping of rough connection interface. Jiang *et al.* (2010) studied the contact stiffness of two rough contact surfaces under different preloads and showed that the relationship between stiffness and contact pressure approximately follows a power law.

There are three finite element analysis methods currently thought to be able to model the contact characteristics of rough interfaces (Bograd *et al.* 2011), i.e. node-to-node contact, thin-layer elements (Ahmadian *et al.* 2006), and zero-thickness elements (Mayer and Gaul 2007). Among them, the thin-layer elements which is also called the virtual material model of joint interface can be conveniently integrated with commercial finite element software. The virtual material method has the advantage of performing finite element analysis of bolted joints with the contact properties of rough interfaces. For instance, Tian *et al.* (2011) applied the virtual material method to model the fixed joint interfaces in machine tools, and the method is verified by modal experiments. The acquisition of virtual material parameters depends on the contact pressure at the interface of bolted joints. However, the interface contact pressure is thought to be uniform distribution on the whole contact area in the present virtual material model, which will result in the homogeneous connection stiffness at the contact interface of bolted joints. This is suitable for very small contact area, but not for a large one and the sparse distribution of bolts.

In this study, the contact pressure distribution at the interface of bolted joints is obtained by using the three-dimensional finite element analysis. The contact surface around bolt is divided into several sub-layers according to the pressure distribution feature, and contact pressure in each sub-layer is assumed to be evenly. The virtual material parameters of each sub-layer can be deduced based on the Hertz contact theory and fractal theory. The virtual materials of all sub-layers are assembled to form a non-uniform virtual material layer, which is then fixed connection with other parts of assembly structure. Finally, the theoretical and experiments are compared by impact response in both time- and frequency-domain, and the effect of surface roughness on dynamic characteristics of bolted joint is also discussed.

2. Non-uniform virtual material model

In this section, a three-dimensional finite element model

for a double-bolted joint is established, on which nonlinear static analysis is implemented to investigate the contact pressure distribution at the joint interface. According to the Hertz contact theory and fractal theory, interface virtual material parameters are derived under contact pressure in different local regions.

2.1 Contact pressure distribution of bolted joint

Assembly structures are usually connected by multiple bolts that arranged at a certain distance. Without losing generality, a double-bolted joint is selected to analyse the contact pressure distribution. The three-dimensional finite element model of a typical double-bolted joint is developed using the finite element analysis software ANSYS as shown in the left part of Fig. 1, where the bolts head and nuts are simplified as cylinders. By neglecting the screw threads contact between bolts and nuts, nodes and elements for the bolts and nuts can be bonded together in the modeling, which not only improves the computation efficiency of finite element model but also has little influence on the analysis result for contact pressure distribution between two plates. All the joint components assume to be homogeneous and isotropic, and the material properties are initially set as the elastic modulus E is 210 GPa, the density is 7850 kg/m³, the Poisson's ratio ν is 0.3. The values of dimensional parameters for the double-bolted joint are illustrated in Fig.1, where the unit is mm. The model contains two identical steel plates with the thickness of 7.5 mm and the bolt hole diameter of 9 mm, while the bolt sizes of M8 are selected to clamp the plates together.

In the finite element model, three contact pairs are defined by surface-to-surface contact using the contact element CONTA174 and the target segment element TARGE170, which are used to the interfaces between bolts head and upper plate, nuts and lower plate, and between the upper plate and lower plate. The friction coefficients of those contact pairs are set to be 0.15. The boundary condition of this model is unilateral fixed in the form of cantilever, i.e. all degrees of freedom of the nodes at the left surface for the lower plate are constrained. The pretension element PRETS179 is utilized to impose the pretightening force on the two bolts.

This model is nonlinear considering the contact between connection components. The nonlinear static analysis of the finite element model is conducted to determine the contact pressure distribution for the double-bolted joint as shown in the middle right part of Fig. 1, where the preload of 5 kN is applied to the two bolts respectively. As can be seen that two circular bands of contact pressure generated by two pretightening bolts are around the two bolt holes respectively. To clearly observe the change of contact pressure in the radial direction of bolt hole, the contact pressure of all nodes on the x -axial are picked up and drawn into a curve as shown in the upper right corner of Fig. 1. It is obviously seen that the contact pressure reaches a peak near the hole edge and drops to zero in a distance to the bolt centerline. The variation feature indicates the non-uniform distribution of contact pressure on the interface of the double-bolted joint.

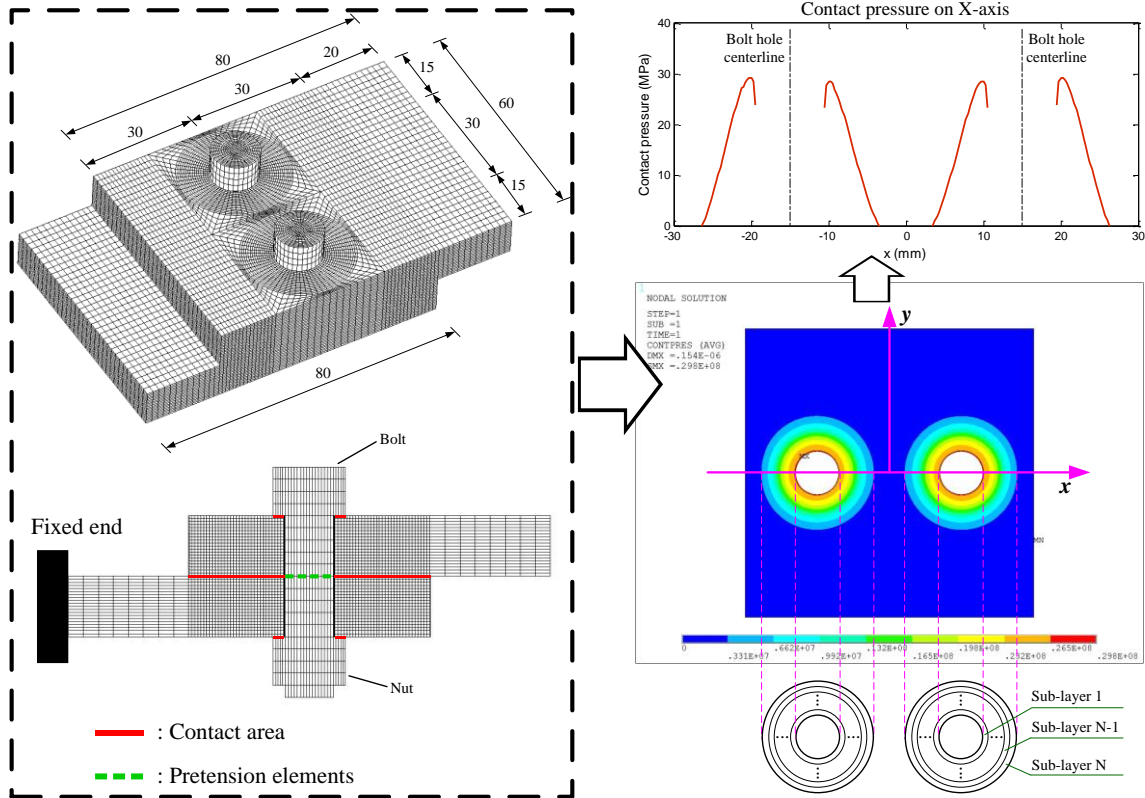


Fig. 1 Finite element model and contact pressure distribution of the double-bolted joint

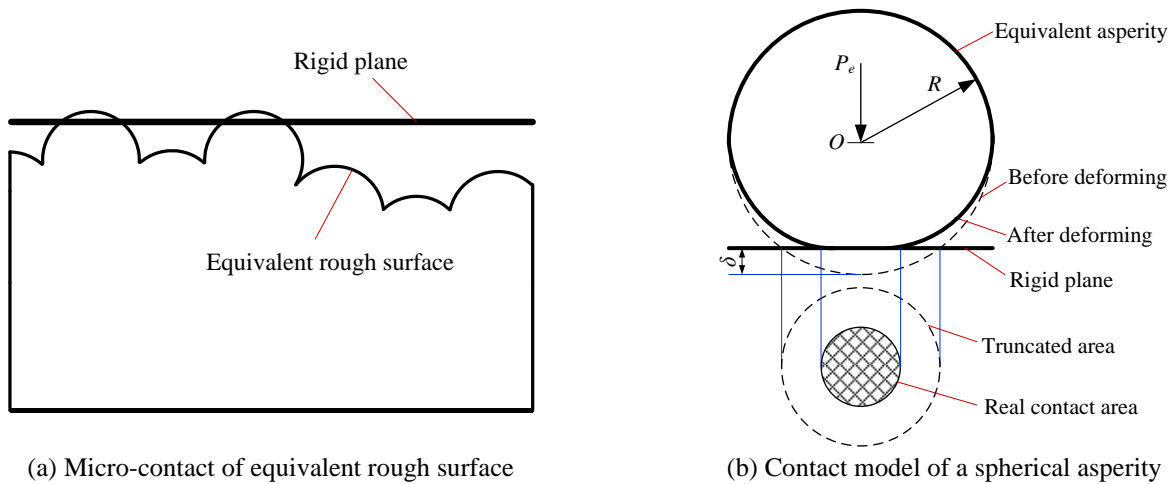


Fig. 2 A simplified contact model for two rough contact surfaces

In order to construct more accurate virtual material on joint interface, the contact surface around the bolt holes is divided into several sub-layers by means of layering thought, as shown in the lower right corner of Fig. 1. Each sub-layer is considered to have evenly contact pressure, which corresponds to virtual material with particular properties. After that, non-uniform virtual material on the joint interface generated by assembling all of the sub-layers, of which material properties are different from each other.

2.2 Analytic model of non-uniform virtual material

A machined surface is always rough at the micro

perspective and composed of randomly distributed asperities. Fractal geometry theory can effectively characterize surfaces with multi-scale roughness with the help of its scale-invariant parameters. The interfacial virtual material properties of rough surfaces for each sub-layer under contact pressure will be derived.

Following the assumption that asperities are spherical near their summits, two rough contact surfaces can be further simplified as a smoothly rigid plane in contact with an equivalent rough surface containing a large number of spherical asperities (Tian *et al.* 2011), as shown in Fig. 2(a). The interaction between a typical asperity and a rigid plane under a normal concentrated force is shown in Fig. 2(b). It

is assumed that the equivalent asperities are far apart from each other and the interaction between the equivalent asperities is negligible. According to the fractal theory, the deforming value δ of the micro-contact equivalent asperity can be given by

$$\delta = G^{D-1} a'^{(1-0.5D)} \quad (1)$$

where D denotes the fractal dimension of contact surface and G represents the fractal roughness parameter of rough surface profile. a' is the truncated area of the micro-contact equivalent asperity.

Considering the geometry of the equivalent asperity before and after elastic deformation and the asperity interference $\delta \ll R$, the relationship between the truncated area a' and equivalent asperity radius R can be expressed as (Tian *et al.* 2011, Zhang *et al.* 2014)

$$a' = 2\pi R\delta \quad (2)$$

Substituting Eq. (2) into Eq. (1), the relation of R and a' can be also written as

$$R = \frac{a'^{0.5D}}{2\pi G^{D-1}} \quad (3)$$

Based on the Hertz contact theory, the normal force P_e imposing on the equivalent asperity at an elastic micro-contact can be expressed as (Zhang *et al.* 2014)

$$P_e = \frac{4}{3} E^* R^{0.5} \delta^{1.5} \quad (4)$$

where E^* is the equivalent elastic modulus of equivalent rough surface and can be obtained by

$$\frac{1}{E^*} = \frac{1-v_1^2}{E_1} + \frac{1-v_2^2}{E_2} \quad (5)$$

in which E_1 , E_2 and v_1 , v_2 are the elastic modulus and Poisson's ratio, respectively.

For the elastic deformation of the equivalent asperity, the stress and strain can be indicated as

$$\sigma = \frac{P_e}{a}, \quad \varepsilon = \frac{\delta}{R} \quad (6)$$

where $a = \pi R\delta$ is the real elastic micro-contact area of equivalent asperity and obtained on the basis of the Hertz contact theory.

Introducing Eq. (4) into Eq. (6) yields

$$\sigma = \frac{4}{3\pi} E^* \sqrt{\frac{\delta}{R}} = \frac{4}{3\pi} E^* \sqrt{\varepsilon} \quad (7)$$

The elastic modulus for a single micro-contact can be obtained by differentiating of Eq. (7), as follows

$$e_e = \frac{d\sigma}{d\varepsilon} = \frac{2}{3\pi} E^* \sqrt{\frac{R}{\delta}} \quad (8)$$

Similarly, the shear modulus of each elastic micro-

contact can be described as

$$g_e = \frac{16}{\pi} G^* \sqrt[3]{1 - \frac{\eta}{\mu}} \quad (9)$$

where η is ratio of tangential load to normal load, μ is the static friction coefficient. G^* refers to the equivalent shear modulus of two contacting rough surfaces with shear moduli G_1 and G_2 , respectively, and can be expressed as

$$\frac{1}{G^*} = \frac{2-v_1}{G_1} + \frac{2-v_2}{G_2} \quad (10)$$

Distinguishing elastic and plastic deformation of the asperities is used by the critical truncated area a'_c that can be written as (Tian *et al.* 2011)

$$a'_c = 2 \left(\frac{2}{q\phi} \right)^{\frac{2}{D-1}} G^2 = 2 \left(\frac{2E^*}{H} \right)^{\frac{2}{D-1}} G^2 \quad (11)$$

where $q=H/\sigma_y$ is the relating factor of rough surface, and $\phi = \sigma_y/E^*$ denotes the material property. H and σ_y are the hardness and yield strength of the softer material, respectively.

The statistical distribution of the truncated area a' for the asperity micro-contact can be taken the form (Wang and Komvopoulos 1994)

$$n(a') = 0.5D\psi^{1-0.5D} a'_L{}^{0.5D} a'^{-1-0.5D} \quad (12)$$

where a'_c denotes the maximum truncated area for asperity elastic micro-contact. ψ represents the domain extension factor of micro-contact size distribution and depends on fractal dimension D , and their relationship is

$$\psi^{1-0.5D} - (1 + \psi^{-0.5D})^{-(2-D)/D} = (2-D)/D \quad (13)$$

When the equivalent asperity is in contact with the rigid flat surface, the state of elastic or plastic deformation of the micro-contact asperity relies on its truncated area. If the truncated area satisfies $a'_c < a' < a'_L$, the micro-contact asperity is in the state of elastic deformation, and the asperity is in plastic deformation regime if it satisfies $a' < a'_c$. For the asperities are in plastic deformation, the normal force P_p , the elastic modulus e_p and shear modulus g_p can be expressed as

$$P_p = 0.5Ha', \quad e_p = g_p = 0 \quad (14)$$

As viewed from macro-contact, the contact pressure of joint interface can be obtained by integrating the distribution of elastic and plastic asperities. Thus, the contact pressure P_i of the i th sub-layer shown in Fig. 1 can be expressed as

$$P_i = \int_0^{a'_c} P_p n(a') da' + \int_{a'_c}^{a'_L} P_e n(a') da' \quad (15)$$

Substituting Eqs. (1)-(4), (12) and (14) into Eq. (15), result in

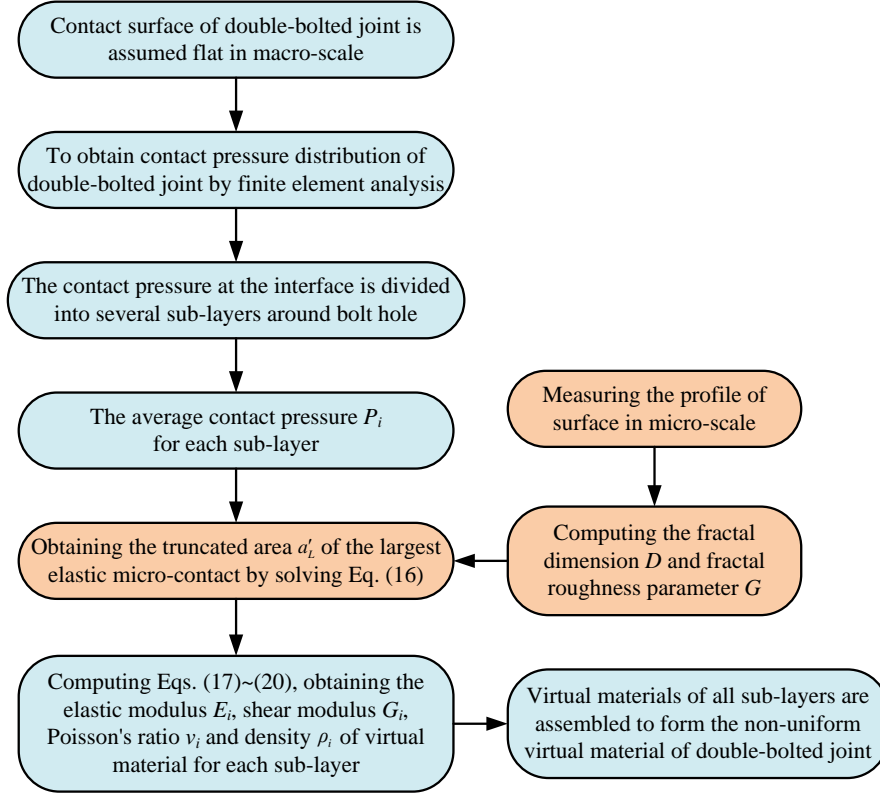


Fig. 3 Flowchart diagram of non-uniform virtual material modeling for double-bolted joint

$$P_i = \begin{cases} D\psi^{1-0.5D} a_L^{0.5D} \left[\frac{0.5Ha_C^{1-0.5D}}{1-0.5D} + \frac{2E^*G^{D-1}(a_L^{1.5-D} - a_C^{1.5-D})}{3\sqrt{2\pi}(1.5-D)} \right] & (D \neq 1.5) \\ 1.5Ha_L^{0.75} a_C^{0.25} \psi^{0.25} + \frac{E^*}{\sqrt{2\pi}} \psi^{0.25} G^{0.5} a_L^{0.75} \ln \frac{a'_L}{a_C} & (D = 1.5) \end{cases} \quad (16)$$

The elastic modulus E_i and shear modulus G_i of virtual material for the i th sub-layer at the joint interface can be obtained by integrating as

$$E_i = \int_{a_C}^{a'_L} e_n(a') a da' / A_i = \frac{2DE^*}{3\pi^2 A_i} \psi^{1-0.5D} G^{1-D} a_L^{0.5D} (a_L^{0.5} - a_C^{0.5}) \quad (17)$$

$$G_i = \int_{a_C}^{a'_L} g_n(a') a da' / A_i = \sqrt{1 - \frac{\eta}{\mu}} \frac{8DG^* \psi^{1-0.5D}}{(2-D)\pi A_i} a_L^{0.5D} (a_L^{1-0.5D} - a_C^{1-0.5D}) \quad (18)$$

where A_i is the nominal interfacial area of the i th sub-layer, and the contact pressure P_i is assumed to be uniformly distributed in the nominal area A_i .

Considering Eqs. (17) and (18), the Poisson's ratio v_i of virtual material for the i th sub-layer at the joint interface shown in Fig. 1 can be calculated as follows

$$v_i = \frac{E_i}{2G_i} - 1 \quad (19)$$

Because the interfacial mass is small compared to the assembly, the density of virtual material has little influence on the dynamic characteristics of bolted joints. A simplified density expression for the virtual material of each sub-layer is

$$\rho_i = \frac{\rho_1 + \rho_2}{2} \quad (20)$$

where ρ_1 and ρ_2 are the densities of two contact surfaces, respectively.

Additionally, the normal contact stiffness K_{ni} and shear contact stiffness K_{ti} of each sub-layer can be expressed by elastic modulus E_i and shear modulus G_i on the basis of Hooke's Law, as follows

$$K_{ni} = E_i A_i / t, \quad K_{ti} = G_i A_i / t \quad (21)$$

where t is the thickness of virtual material layer.

At this point, the virtual materials properties containing elastic modulus, shear modulus, Poisson's ratio and density for all sub-layers at the joint interface of double-bolted joint are determined on the basis of fractal topography theory. The flowchart diagram for the determination of virtual material properties is depicted in Fig. 3. To begin with, the contact surfaces of bolted joint is considered to be flat in the macro-scale, and contact pressure distribution can be obtained by finite element analysis. The contact interface is divided into several sub-layers, in which the contact pressure is assumed to be uniformly distributed. For each

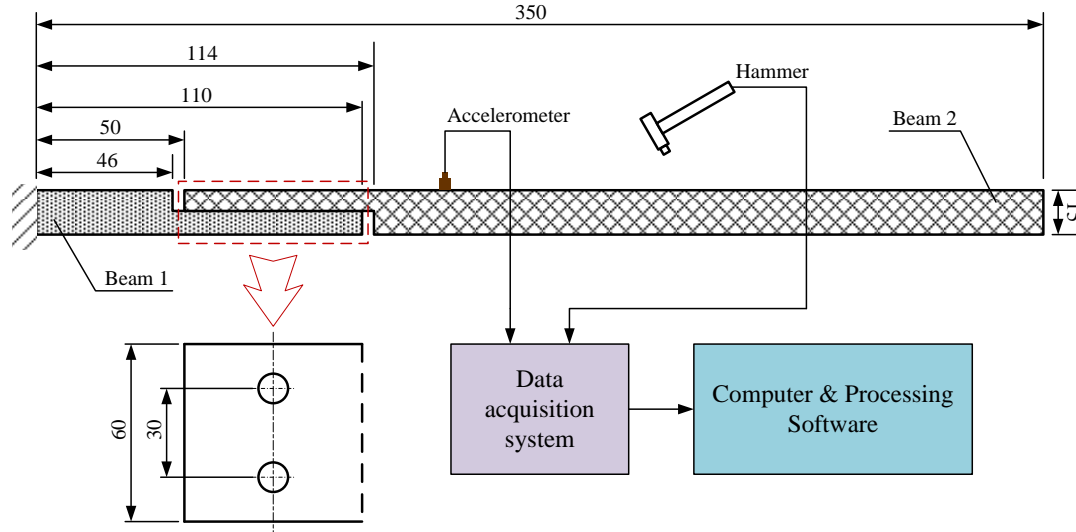


Fig. 4 Mesh grid of topographic model

sub-layer, the relationship between contact pressure and virtual material parameters can be established through the truncated area of largest elastic micro-contact a'_L . Ultimately, virtual materials with different properties for all sub-layers are assembled to form the non-uniform virtual material on the joint interface of bolted joints.

2.3 Determination of fractal parameters

The fractal dimension D and fractal roughness parameter G are two fractal parameters that need to be determined by measuring the profile of rough contact surface in micro-scale. Mathematical expression of rough surface profile usually adopts the Weierstrass-Mandelbrot (W-M) function, which can be written as

$$z(x) = L \left(\frac{G}{L} \right)^{D-1} \sum_{n=0}^{\infty} \frac{\cos(2\pi\gamma^n x/L)}{\gamma} \quad (22)$$

where x is the lateral distance, $z(x)$ is the height of surface profile, L is the length of fractal sample, while γ denotes the scaling parameter that can be used to obtain the spectral density and self-affine property.

The structure function $S(\tau)$ of the W-M function can be expressed as (Jiang *et al.* 2010)

$$S(\tau) = \left\langle [z(x) - z(x + \tau)]^2 \right\rangle = C\tau^{4-2D} \quad (23)$$

where τ is the displacement, $\langle \rangle$ represents the average value of the statistical along the x -direction, and C denotes scaling coefficient and can be given by

$$C = \frac{\Gamma(2D-3)}{2-D} G^{2(D-1)} \sin\left(\frac{2D-3}{2}\pi\right) \quad (24)$$

In the double logarithmic coordinates, Eq. (23) can be rewritten as

$$\log S(\tau) = (4-2D)\log\tau + \log C \quad (25)$$

It is found that the plot of $\log S(\tau)$ as a function of $\log\tau$ in Eq. (25) is a straight line, and the fractal dimension D is relate to the slope k of the straight line, while the fractal roughness parameter C can reflect the intercept b of the straight line. Thus, the fractal parameters can be obtained by

$$D = 2 - 0.5k \quad (26)$$

$$G = \left[\frac{10^b (2-D)}{\Gamma(2D-3) \sin\left(\frac{2D-3}{2}\pi\right)} \right]^{\frac{1}{2(D-1)}} \quad (27)$$

When two rough contact rough surfaces are equivalent to a rough surface and a rigid plane, the structure function of the equivalent rough surface is calculated by the structure functions of two rough contact surfaces, and their relationship as

$$S_{eq}(\tau) = S_1(\tau) + S_2(\tau) \quad (28)$$

where $S_1(\tau)$ and $S_2(\tau)$ are the structure functions of two contact surfaces, respectively.

3. Experiment validation of non-uniform virtual material model

3.1 Experiment set-up

In order to verify the proposed contact pressure distribution based non-uniform virtual material model, the beam lap structure with double-bolted joint is designed as shown in Fig. 4, where dimensions and configurations are illustrated and the unit is mm. The diameter of bolt hole is 9 mm. Two beams namely beam 1 and beam 2 are connected by two bolts, which sizes are M8 with grade 8.8. The left

Table 1 Mechanical properties of two connected beams

Parameter	Value
Young's modulus (GPa)	210
Poisson's ratio	0.3
Density (kg/m ³)	7850
Hardness (MPa)	500
Yield strength (MPa)	350

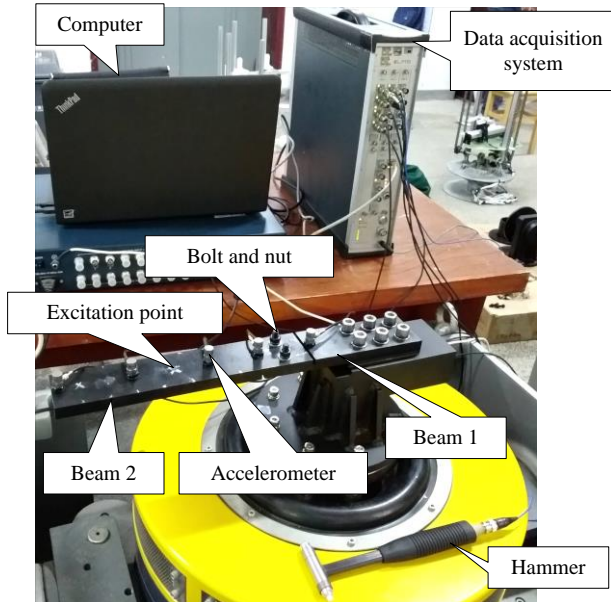


Fig. 5 Experimental set-up of beam lap structure with double-bolted joint

end of beam 1 is fixed to form a cantilever beam for the beam lap structure. The two beams are manufactured of 45# steel, and their material properties are listed in Table 1. Overlap area of the assembled structure is 60×60 mm. In fact, the dimensions and materials of the overlap joint shown in Fig. 4 are identical with that of Fig. 1. The finish milling processing is applied to the contact surfaces with roughness $R_a = 0.2 \mu\text{m}$.

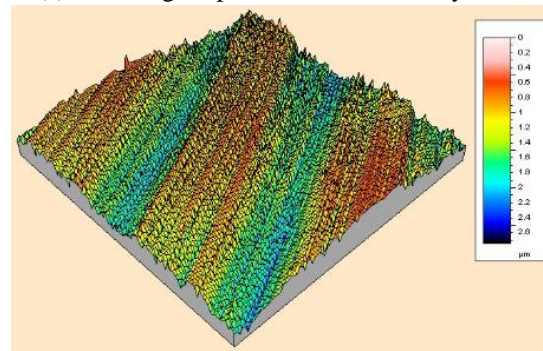
Experimental set-up of test system for the assembly structure is shown in Fig. 5. Five piezoelectric acceleration sensors are placed on the two beams to collect the vibration response signals. An impact hammer is utilized for excitation, and the excitation point is located at the mid-span of beam 2. The data acquisition instrument LMS is adopted to collect the signals from the sensors and impact hammer. In the experiment, the torque wrench is used to control the value of tightening torque, and then the tightening torque applied to the bolt is converted to a pretension force. The relationship between the tightening torque T and pretension force F can be described as $T=0.2dF$, where d is the nominal diameter of bolt.

3.2 Experiment validation

The tightening torque of 8 Nm is applied to the two bolts, respectively, resulting in the preload of 5 kN for each bolt. Since the experimental double-bolted joint is the same



(a) White-light optical interferometer system



(b) Measured three-dimensional surface profile

Fig. 6 Talysurf CCI 6000 white-light optical interferometer system and measured three-dimensional surface profile

as that in Section 2.1, the contact pressure distribution shown in Fig. 1 will be used to determine the non-uniform virtual material of joint interface for the experimental assembled structure.

In the micro-scale, the rough surface profile is measured by the Talysurf CCI 6000 white-light optical interferometer system for obtaining the fractal parameters of the rough contact surface, as shown in Fig. 6, where the sampling area of rough surface profile is 360×360 μm . According to Eq. (23), the structure function of the rough surface profile can be obtained. In the double logarithmic coordinates, the structure function of the profile is depicted in Fig. 7. The least squares method is employed for linear fitting of the structure function. The fractal dimension and fractal rough parameter of the equivalent rough surface are subsequently determined as $D_{\text{eq}} = 1.69$, $G_{\text{eq}} = 2.4261 \times 10^{-9} \text{ m}$ in the light of Eqs. (26)-(28).

In order to improve the calculation efficiency, the contact pressure distribution produced by each bolt is divided into five sub-layers (i.e., $N = 5$). According to flowchart diagram of the Fig. 3, the property parameters of virtual material in each sub-layer can be derived, and are listed in Table 2. The virtual material layer is used to describe the mechanical behaviors of joint interface, and is fixedly connected with the two beams. Finite element

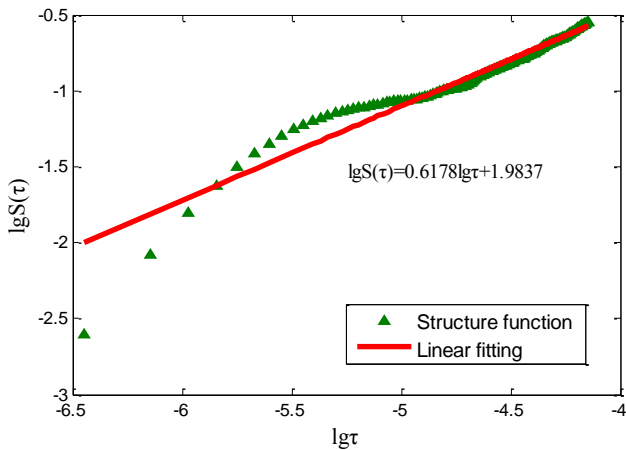


Fig. 7 Structure function and its linear fitting function for the measured surface profile

Table 2 Virtual material properties for each sub-layer

Sub-layer number	1	2	3	4	5
Contact force (N)	1845.3	1665.4	984.3	409	96
Elastic modulus (GPa)	24.5	16.2	7.39	2.42	0.45
Shear modulus (GPa)	20.2	13.3	6.09	2.00	0.37
Poisson's ratio	-0.39	-0.39	-0.39	-0.39	-0.39
Density (kg/m ³)	7850	7850	7850	7850	7850

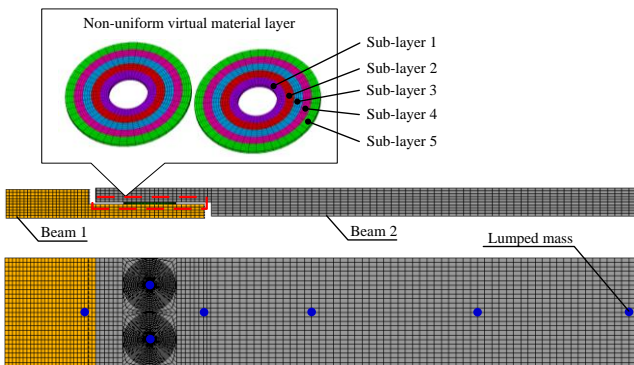


Fig. 8 Finite element model containing non-uniform virtual material

dynamic model for the beam lap structure with double-bolted joint is developed as shown in Fig. 8, where the thickness of the non-uniform virtual material layer is 1 mm. In the finite element model, the two bolt holes are filled with actual bolt material to ensure the bolt stiffness, and bolt heads, nuts, and accelerometers are included in the model and replaced by the lumped mass applied on the nodes. The MASS21 element in ANSYS software is used to define the lumped mass, which is set to 20 g for each one in the model.

For the sake of validating the effectiveness of proposed method, the simulated vibration response in time-domain and frequency-domain are compared with that of experiment results from impact excitation of hammer. The hammer excitation is performed manually at a 135 mm away for the free end of beam 2. A detailed view of measured input force in the experiment and the synthesized

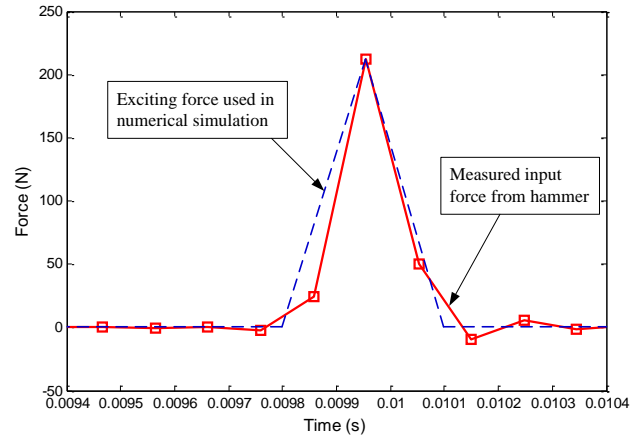


Fig. 9 A detailed view of measured input force and exciting force used for numerical simulation

exciting force used for numerical simulation are shown in Fig. 9. The collected data from the accelerometer that is mounted on the beam 2 near the bolts. The comparison of experiment results and simulation results of vibration response in time-domain for the assembly structure is displayed in Fig. 10(a). As can be seen that the numerical simulation results show good correspondence with experiment results. Frequency response can be obtained by fast Fourier transform of vibration response in time-domain, and the comparison results in frequency-domain is show in Fig. 10(b). The computational and experimental results agree fairly well, which validates the effectiveness of proposed non-uniform virtual material method. Furthermore, it is observed that response amplitude of simulation results is a little larger than that of experimental results in both time- and frequency-domain. This phenomenon is mainly caused by setting errors of exciting force and damping ratio.

To illustrate the accuracy of proposed method, three other approaches, i.e. the bonded assembly, the pre-stressed modal analysis, and the uniform virtual material, are introduced for comparison with the presented non-uniform virtual material. For the bonded assembly, the nodes and elements of the joint interface are fixed together, which means ignoring the effect of contact surface on dynamic characteristics. The pre-stressed modal analysis takes two steps to complete, the static structural analysis considering the frictional contact is first implemented to generate stress and strain of structure, which as initial condition for next modal analysis. For the uniform virtual material, the contact pressure at the joint interface is assumed to be evenly distributed. The value of contact pressure is equal to the sum of pretension force of two bolts for the double-bolted joint, i.e. $P_{total} = 10$ kN, and the corresponding property parameters of virtual material for the uniform case are $E_z = 2.62$ GPa and $G_{xy} = 2.16$ GPa.

The first four natural frequencies of the assembly structure adopting experiment and different approaches are illustrated in Table 3, where the experimental natural frequencies are obtained by hammering impact testing method. In order to reduce random error and improve signal-to-noise ratio, the average results of five trials are

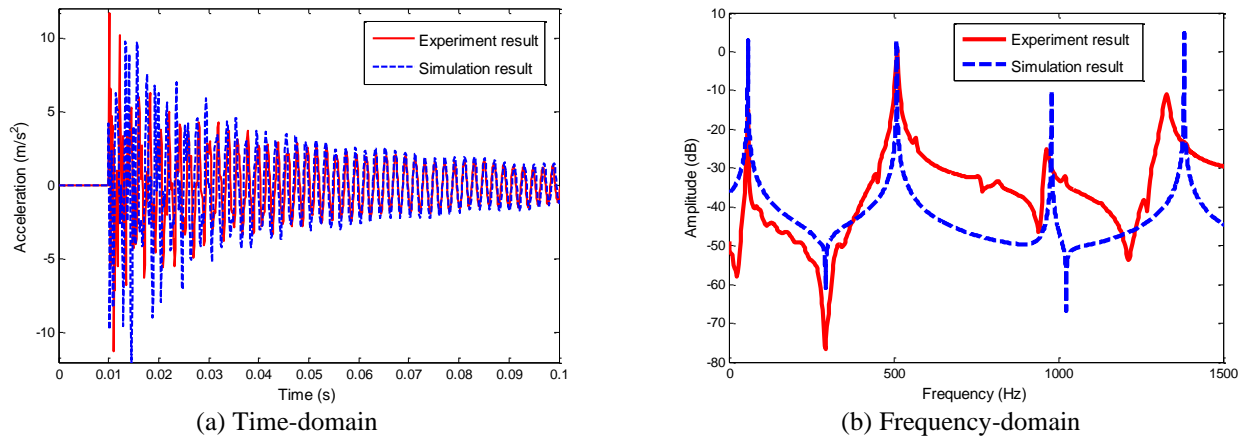


Fig. 10 Comparison of experiment results and simulation results for impulse response in time-domain and frequency-domain

used as the final experimental natural frequencies. The beam lap structure also needs to be disassembled and assembled five times in the experiment. As can be seen in Table 3, the errors of natural frequencies calculated by the bonded assembly method are relatively large due to the neglect of the joint interface. Although the pre-stressed modal analysis method considering initial static stress and strain decreases errors to a certain extent, the errors of first two natural frequencies are up to 24.65% and 10.76%, respectively. The maximum error for the uniform virtual material method appears at the first order with an error of 20.07%, which still affects the accuracy of dynamic analysis for the joint structure. From the calculation results of the previous three methods, it can be observed that the contact interface of the double-bolted joint has a significant effect on the first-order natural frequencies. For the proposed non-uniform virtual material, the errors of first four natural frequencies are -0.02%, -0.04%, 0.53% and 0.52%, respectively, which obviously reduces errors by comparing with the remaining three other methods. It should be emphasized here that the accuracy of proposed method depends on the division number of sub-layer of non-uniform virtual material on the joint interface. The accuracy improve with the number of divisions. Thus, contact pressure distribution of bolted joint must be considered to construct an accurate dynamic model. The presented non-uniform virtual material modeling method on contact interface can satisfy the accuracy requirement for predicting the dynamic characteristics of the assembly structure with bolted joints.

3.3 Discussion

In the micro-scale, the contact surfaces of bolted joints are always rough and composed of randomly distributed asperities. Consequently, rough contact surfaces is one of the main factors affecting the dynamic characteristics of joint structure. The rough surface can be described by the two fractal parameters, i.e. fractal dimension D and fractal roughness parameter G , on the basis of fractal geometry theory. Understanding the influence of surface roughness on the dynamic characteristics can be achieved by the two fractal parameters.

Table 3 Comparison of the first four-order natural frequencies for the double-bolted joint beam under different methods

Natural frequencies (Hz)	f_1	f_2	f_3	f_4
Experimental results	57.5	507.5	970	1323
Bonded assembly	77.14	566.45	988.19	1549.70
Pre-stressed modal analysis	71.68	562.09	911.54	1384.40
Uniform virtual material	69.04	549.15	931.77	1354.80
Non-uniform virtual material	57.49	507.25	975.13	1329.85
Error of bonded assembly (%)	34.15	11.62	1.88	17.14
Error of pre-stressed modal analysis (%)	24.65	10.76	-6.03	4.64
Error of uniform virtual material (%)	20.07	8.21	-3.94	2.40
Error of non-uniform virtual material (%)	-0.02	-0.04	0.53	0.52

Tightening torques of 8 Nm, 12 Nm and 16 Nm, i.e. the corresponding pretension force are 5 kN, 7.5 kN and 10 kN, are applied to the assembly structure shown in Fig.4 respectively. Then, by introducing different values of fractal dimension D and fractal roughness parameter G , the different properties of non-uniform virtual material layer are acquired, and finite element model shown in Fig. 8 is used to calculate the dynamic parameters. The relationships between first four natural frequencies and fractal dimension under different tightening torques are illustrated in Fig. 11. It can be seen that the natural frequency of each order is improved with the increase of tightening torque and fractal dimension, which indicates that the stiffness of bolted joints is affected by contact pressure and rough contact surfaces. Actually, increasing the fractal dimension implies that the contact surface becomes smoother and the contact stiffness of joint interface is improved as shown in Fig. 12, where the normal stiffness and shear stiffness for each sub-layer of the non-uniform virtual material layer are increased with the fractal dimension. When the value of fractal dimension is big enough, the natural frequency of each order shown in Fig. 11 change very little. The first and second order natural frequencies increase slightly with the fractal dimension,

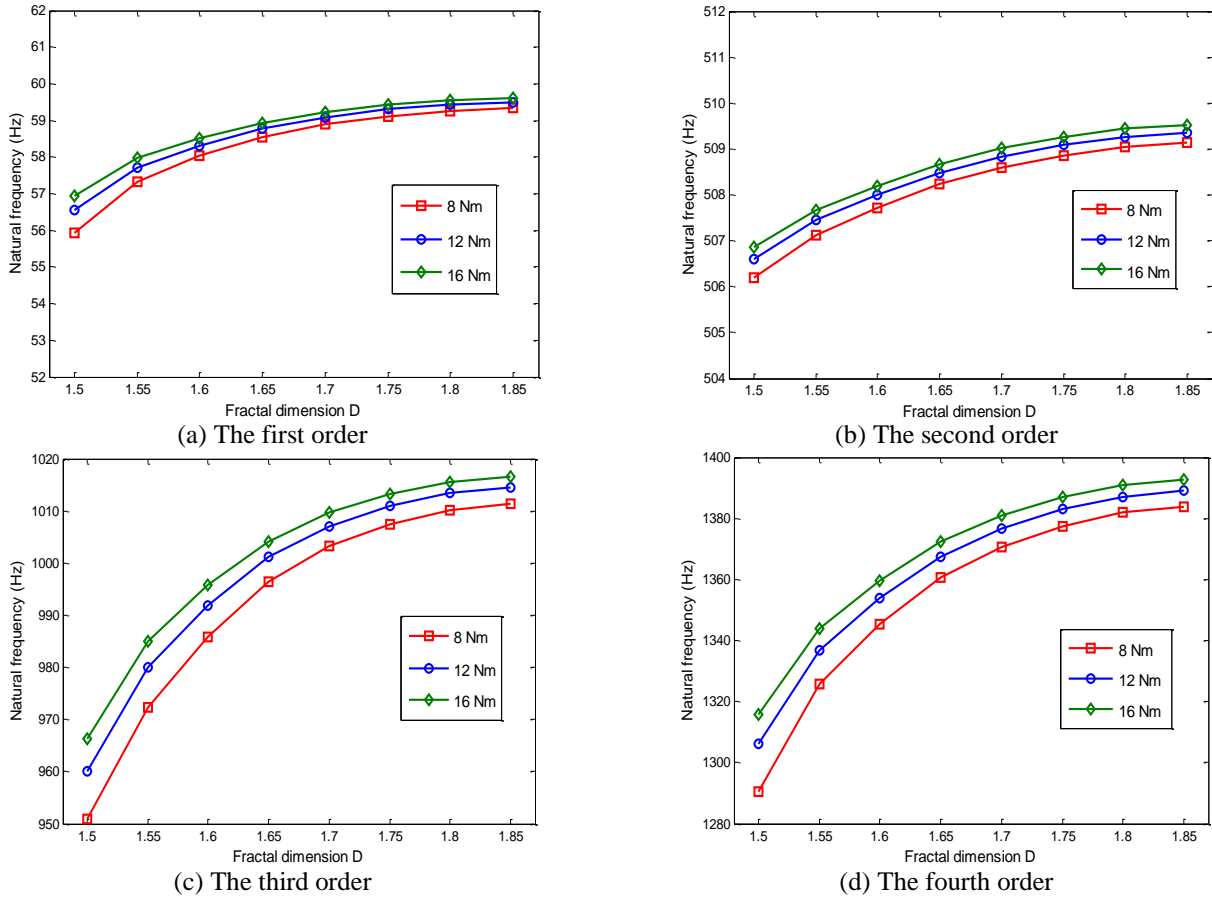


Fig. 11 Relationships between first four natural frequencies and fractal dimension under different tightening torques

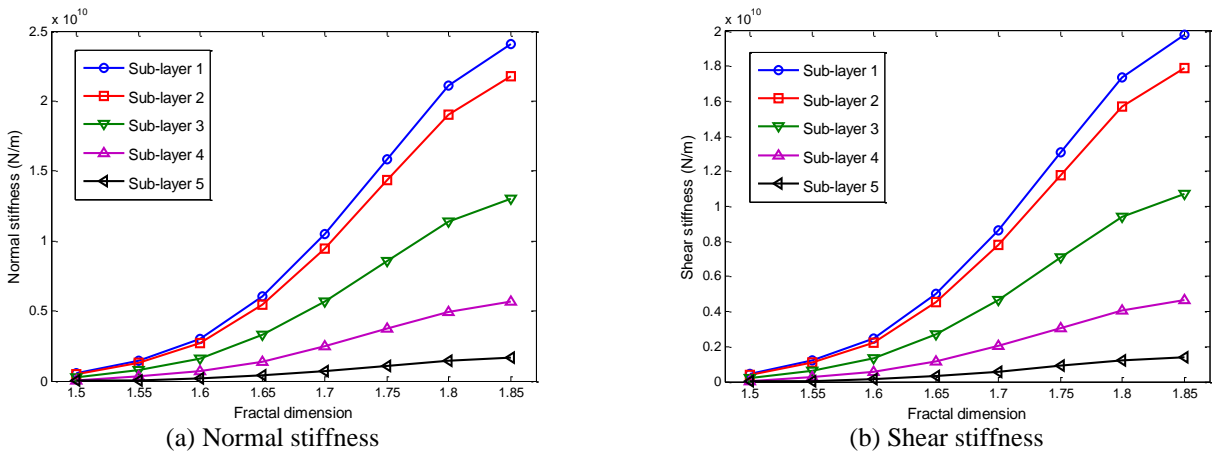


Fig. 12 Effect of the fractal dimension on normal stiffness and shear stiffness for each sub-layer of the non-uniform virtual material layer

which means the fractal dimension has little effect on the low-order natural frequencies.

Keeping other structural parameters unchanged, the relationships between the first four natural frequencies and fractal roughness parameter for different levels of the tightening torque are shown in Fig. 13. The increase of the fractal roughness parameter means that the contact surface is rougher, which leads to the decrease of contact stiffness as shown in Fig. 14. Thus, the first four natural frequencies shown in Fig. 13 are cut down along with the increase of the fractal roughness parameter. Meanwhile, it is more

obviously to distinguish the natural frequencies under different tightening torques. Similar to the fractal dimension, the influence of the fractal roughness parameter on low-order natural frequencies is small.

4. Conclusions

A contact pressure distribution based non-uniform virtual material model on contact interface has been developed for dynamic analysis of bolted joints. The

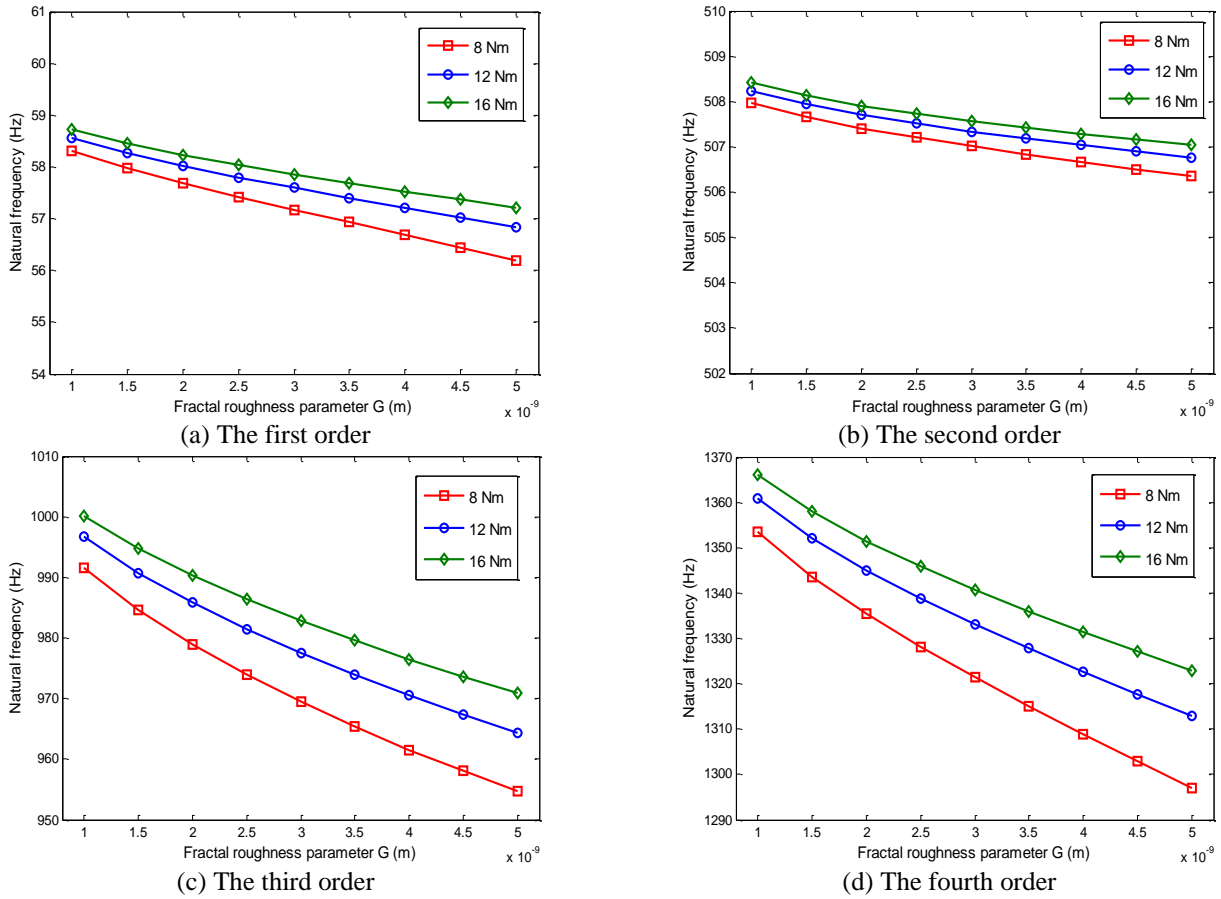


Fig. 13 Relationships between first four natural frequencies and fractal roughness parameter under different tightening torques

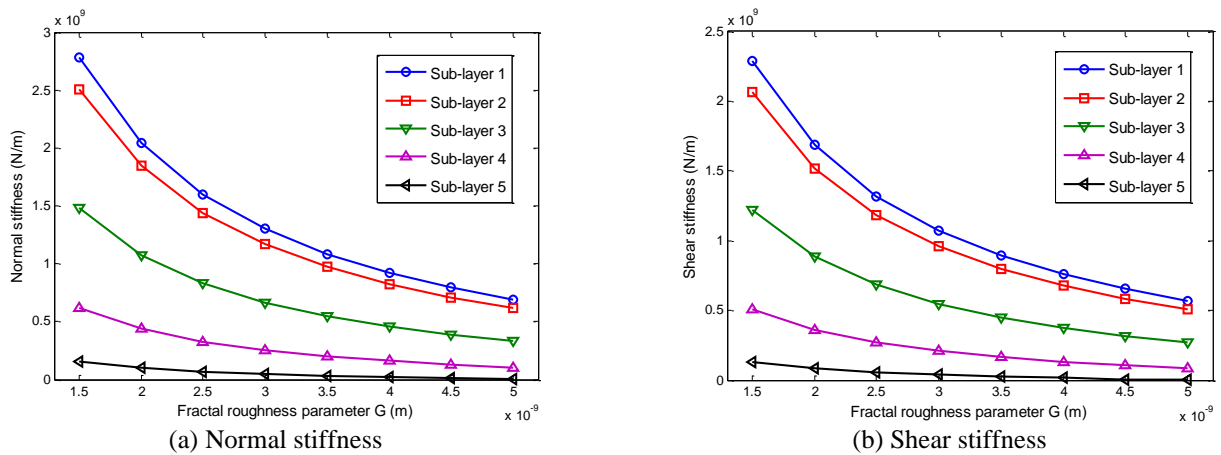


Fig. 14 Effect of the fractal roughness parameter on normal stiffness and shear stiffness for each sub-layer of the non-uniform virtual material layer

proposed method can be applied to multi-bolt connection structure with sparse bolt distribution. The contact pressure distribution of bolted joints was first obtained by the nonlinear static analysis in the finite element software ANSYS. The contact surface around bolt was divided into several sub-layers, and contact pressure in each sub-layer was considered to be evenly. Using the virtual material hypothesis and fractal contact theory, the relationship between contact pressure and virtual material properties for

each sub-layer was established. The theoretical results were compared with experimental results by impact response in both time- and frequency-domain. It was found that theoretical results were in good agreement with experimental results, and the maximum error of the first four natural frequencies was within 1%, which validated the effectiveness of the proposed method. The influence of rough contact surfaces on dynamic characteristics of bolted joints was also discussed, and the smoother contact surfaces

can improve the contact stiffness, whereas it had little effect on the low-order natural frequencies.

Acknowledgments

The research described in this paper was financially supported by Science Challenge Project (No. TZ2018007) and National Natural Science Foundation of China (No. 51775410).

References

- Abad, J., Franco, J.M., Celorrio, R. and Lezaun, L. (2012), "Design of experiments and energy dissipation analysis for a contact mechanics 3D model of frictional bolted lap joints", *Adv. Eng. Soft.*, **45**(1), 42-53. <https://doi.org/10.1016/j.advengsoft.2011.09.021>.
- Adel, F., Shokrollahi, S., Jamal-Omidi, M., Ahmadian, H. (2017), "A model updating method for hybrid composite/aluminum bolted joints using modal test data", *J. Sound Vib.*, **396**, 172-185. <https://doi.org/10.1016/j.jsv.2017.02.035>.
- Abid, M. and Khan, Y.M. (2013), "The effect of bolt tightening methods and sequence on the performance of gasketed bolted flange joint assembly", *Struct. Eng. Mech.*, **46**(6), 843-852. <https://doi.org/10.12989/sem.2013.46.6.843>.
- Ahmadian, H. and Jalali, H. (2007a), "Identification of bolted lap joints parameters in assembled structures", *Mech. Syst. Signal Pr.*, **21**(2), 1041-1050. <https://doi.org/10.1016/j.ymsp.2005.08.015>.
- Ahmadian, H. and Jalali, H. (2007b), "Generic element formulation for modelling bolted lap joints", *Mech. Syst. Signal Pr.*, **21**(5), 2318-2334. <https://doi.org/10.1016/j.ymsp.2006.10.006>.
- Ahmadian, H., Mottershead, J.E., James, S., Friswell, M.I. and Reece, C.A. (2006), "Modelling and updating of large surface-to-surface joints in the AWE-MACE structure", *Mech. Syst. Signal Pr.*, **20**(4), 868-880. <https://doi.org/10.1016/j.ymsp.2005.05.005>.
- Argatov, II. and Bucher, E.A. (2011), "On the Iwan models for lap-type bolted joints", *Int. J. Nonlin. Mech.* **46**(2), 347-356. <https://doi.org/10.1016/j.ijnonlinmec.2010.09.018>.
- Bograd, S., Reuss, P., Schmidt, A., Gaul, L. and Mayer, M. (2011), "Modeling the dynamics of mechanical joints", *Mech. Syst. Signal Pr.*, **25**(8), 2801-2826. <https://doi.org/10.1016/j.ymsp.2011.01.010>.
- Brake, M.R.W. (2017), "A reduced Iwan model that includes pinning for bolted joint mechanics", *Nonlinear Dynam.*, **87**(2), 1335-1349. <https://doi.org/10.1007/s11071-016-3117-2>.
- Gant, F., Rouch, P., Louf, F. and Champaney, L. (2011), "Definition and updating of simplified models of joint stiffness", *Int. J. Solids Struct.*, **48**(5), 775-784. <https://doi.org/10.1016/j.ijsolstr.2010.11.011>.
- Greenwood, J.A. and Williamson, J.B.P. (1966), "The contact of nominally-flat surfaces", *Proc. R. Soc. London A*, **295**(1442), 300-319. [https://doi.org/10.1016/0043-1648\(67\)90287-6](https://doi.org/10.1016/0043-1648(67)90287-6).
- Heller, L., Foltête, E. and Piranda, J. (2009), "Experimental identification of nonlinear dynamic properties of built-up structures", *J. Sound Vib.*, **327**(1-2), 183-196. <https://doi.org/10.1016/j.jsv.2009.06.008>.
- Iranzad, M. and Ahmadian, H. (2012), "Identification of nonlinear bolted lap joint models", *Comput. Struct.*, **96-97**, 1-8. <https://doi.org/10.1016/j.compstruc.2012.01.011>.
- Jackson, R.L. and Green, I. (2005), "A finite element study of elasto-plastic hemispherical contact against a rigid flat", *J. Tribol-T ASME*, **127**(2), 343-354. <https://doi.org/10.1115/1.1866166>.
- Jiang, S., Zheng, Y. and Zhu, H. (2010), "A contact stiffness model of machined plane joint based on fractal theory", *J. Tribol-T ASME*, **132**, 011401. <https://doi.org/10.1115/1.4000305>.
- Kim, J., Yoon, J.C. and Kang, B.S. (2007), "Finite element analysis and modeling of structure with bolted joints", *Appl. Math. Model.*, **31**(5), 895-911. <https://doi.org/10.1016/j.apm.2006.03.020>.
- Kogut, L. and Etsion, I. (2002), "Elastic-Plastic Contact Analysis of a Sphere and a Rigid Flat", *J. Appl. Mech-T ASME*, **69**(5), 657-662. <https://doi.org/10.1115/1.1490373>.
- Ksentini, O., Combes, B., Abbes, M.S., Daidie, A. and Haddar, M. (2015), "Simplified model to study the dynamic behaviour of a bolted joint and its self loosening", *Struct. Eng. Mech.*, **55**(3), 639-654. <https://doi.org/10.12989/sem.2015.55.3.639>.
- Lopez-Arancibia, A., Altuna-Zugatis, A.M., Aldasoro, H.A. and Pradera-Mallabiarrena, A. (2015), "Bolted joints for single-layer structures: numerical analysis of the bending behaviour", *Struct. Eng. Mech.*, **56**(3), 355-367. <https://doi.org/10.12989/sem.2015.56.3.355>.
- Mayer, M.H. and Gaul, L. (2007), "Segment-to-segment contact elements for modelling joint interfaces in finite element analysis", *Mech. Syst. Signal Pr.*, **21**(2), 724-734. <https://doi.org/10.1016/j.ymsp.2005.10.006>.
- Majumdar, A. and Bhushan, B. (1991), "Fractal model of elastic-plastic contact between rough surfaces", *J. Tribol-T ASME*, **113**(1), 1-11. <https://doi.org/10.1115/1.2920588>.
- Mehrpouya, M., Graham, E. and Park, S.S. (2013), "FRF based joint dynamics modeling and identification", *Mech. Syst. Signal Pr.*, **39**(1-2), 265-279. <https://doi.org/10.1016/j.ymsp.2013.03.022>.
- Mignolet, M.P., Song, P. and Wang, X.Q. (2015), "A stochastic Iwan-type model for joint behavior variability modeling", *J. Sound Vib.*, **349**, 289-298. <https://doi.org/10.1016/j.jsv.2015.03.032>.
- Song, Y., Hartwigsen, C.J., McFarland, D.M., Vakakis, A.F. and Bergman L.A. (2004), "Simulation of dynamics of beam structures with bolted joints using adjusted Iwan beam elements", *J. Sound Vib.*, **273**(1), 249-276. [https://doi.org/10.1016/s0022-460x\(03\)00499-1](https://doi.org/10.1016/s0022-460x(03)00499-1).
- Tian, H., Li, B., Liu, H., Mao, K., Peng, F. and Huang, X. (2011), "A new method of virtual material hypothesis-based dynamic modeling on fixed joint interface in machine tools", *Int. J. Mach. Tool. Manu.*, **51**(3), 239-249. <https://doi.org/10.1016/j.ijmachtools.2010.11.004>.
- Wang, S. and Komvopoulos, K. (1994), "A fractal theory of the interfacial temperature distribution in the slow sliding regime: Part I-elastic contact and heat transfer analysis", *J. Tribol-T ASME*, **116**(4), 812-822. <https://doi.org/10.1115/1.2927338>.
- Zhang, X., Wang, N., Lan, G., Wen, S. and Chen, Y. (2014), "Tangential damping and its dissipation factor models of joint interfaces based on fractal theory with simulation", *J. Tribol-T ASME*, **136**(1), 011704. <https://doi.org/10.1115/1.4025548>.